. .

Search for Neutrinoless Double-Beta Decay of ^{130}Te with CUORE-0

K. Alfonso,[1] D. R. Artusa,[2,3] F. T. Avignone III,[2] O. Azzolini,[4] M. Balata,[3] T. I. Banks,[5,6] G. Bari,[7] J.W. Beeman,[8] F. Bellini,[9,10] A. Bersani,[11] M. Biassoni,[12,13] C. Brofferio,[12,13] C. Bucci,[3] A. Caminata,[11] L. Canonica,[3] X. G. Cao,[14] S. Capelli,[12,13] L. Cappelli,[3,15] L. Carbone,[13] L. Cardani,[9,10,*] N. Casali,[9,10] L. Cassina,[12,13] D. Chiesa,[12,13] N. Chott,[2] M. Clemenza,[12,13] S. Copello,[16,11] C. Cosmelli,[9,10] O. Cremonesi,[13] R. J. Creswick,[2] J. S. Cushman,[17] I. Dafinei,[10] A. Dally,[18] S. Dell'Oro,[3,19] M. M. Deninno,[7] S. Di Domizio,[16,11] M. L. Di Vacri,[3,20] A. Drobizhev,[5,6] L. Ejzak,[18] D. Q. Fang,[14] M. Faverzani,[12,13] G. Fernandes,[16,11] E. Ferri,[12,13] F. Ferroni,[9,10] E. Fiorini,[13,12] S. J. Freedman,[6,5,†] B. K. Fujikawa,[6] A. Giachero,[12,13] L. Gironi,[12,13] A. Giuliani,[21] P. Gorla,[3] C. Gotti,[12,13] T. D. Gutierrez,[22] E. E. Haller,[8,23] K. Han,[17,6] E. Hansen,[24,1] K. M. Heeger,[17] R. Hennings-Yeomans,[5,6] K. P. Hickerson,[1] H. Z. Huang,[1] R. Kadel,[25] G. Keppel,[4] Yu. G. Kolomensky,[5,25] K. E. Lim,[17] X. Liu,[1] Y. G. Ma,[14] M. Maino,[12,13] M. Martinez,[9,26] R. H. Maruyama,[17] Y. Mei,[6] N. Moggi,[27,7] S. Morganti,[10] S. Nisi,[3] C. Nones,[28] E. B. Norman,[29,30] A. Nucciotti,[12,13] T. O'Donnell,[5,6] F. Orio,[10] D. Orlandi,[3] J. L. Ouellet,[5,6] C. E. Pagliarone,[3,15] M. Pallavicini,[16,11] V. Palmieri,[4] L. Pattavina,[3] M. Pavan,[12,13] M. Pedretti,[29] G. Pessina,[13] V. Pettinacci,[10] G. Piperno,[9,10] S. Pirro,[3] S. Pozzi,[12,13] E. Previtali,[13] C. Rosenfeld,[2] C. Rusconi,[13] E. Sala,[12,13] S. Sangiorgio,[29] D. Santone,[3,20] N. D. Scielzo,[29] M. Sisti,[12,13] A. R. Smith,[6] L. Taffarello,[31] M. Tenconi,[21] F. Terranova,[12,13] C. Tomei,[10] S. Trentalange,[1] G. Ventura,[32,33] M. Vignati,[10] S. L. Wagaarachchi,[5,6] B. S. Wang,[29,30] H. W. Wang,[14] L. Wielgus,[18] J. Wilson,[2] L. A. Winslow,[24] T. Wise,[17,18] L. Zanotti,[12,13] C. Zarra,[3] G. Q. Zhang,[14] B. X. Zhu,[1] and S. Zucchelli[34,7]

(CUORE Collaboration)

[1] *Department of Physics and Astronomy, University of California, Los Angeles, CA 90095 - USA*
[2] *Department of Physics and Astronomy, University of South Carolina, Columbia, SC 29208 - USA*
[3] *INFN - Laboratori Nazionali del Gran Sasso, Assergi (L'Aquila) I-67010 - Italy*
[4] *INFN - Laboratori Nazionali di Legnaro, Legnaro (Padova) I-35020 - Italy*
[5] *Department of Physics, University of California, Berkeley, CA 94720 - USA*
[6] *Nuclear Science Division, Lawrence Berkeley National Laboratory, Berkeley, CA 94720 - USA*
[7] *INFN - Sezione di Bologna, Bologna I-40127 - Italy*
[8] *Materials Science Division, Lawrence Berkeley National Laboratory, Berkeley, CA 94720 - USA*
[9] *Dipartimento di Fisica, Sapienza Università di Roma, Roma I-00185 - Italy*
[10] *INFN - Sezione di Roma, Roma I-00185 - Italy*
[11] *INFN - Sezione di Genova, Genova I-16146 - Italy*
[12] *Dipartimento di Fisica, Università di Milano-Bicocca, Milano I-20126 - Italy*
[13] *INFN - Sezione di Milano Bicocca, Milano I-20126 - Italy*
[14] *Shanghai Institute of Applied Physics, Chinese Academy of Sciences, Shanghai 201800 - China*
[15] *Dipartimento di Ingegneria Civile e Meccanica, Università degli Studi di Cassino e del Lazio Meridionale, Cassino I-03043 - Italy*
[16] *Dipartimento di Fisica, Università di Genova, Genova I-16146 - Italy*
[17] *Department of Physics, Yale University, New Haven, CT 06520 - USA*
[18] *Department of Physics, University of Wisconsin, Madison, WI 53706 - USA*
[19] *INFN - Gran Sasso Science Institute, LAquila I-67100 - Italy*
[20] *Dipartimento di Scienze Fisiche e Chimiche, Università dell'Aquila, L'Aquila I-67100 - Italy*
[21] *Centre de Sciences Nucléaires et de Sciences de la Matière (CSNSM), 91405 Orsay Campus - France*
[22] *Physics Department, California Polytechnic State University, San Luis Obispo, CA 93407 - USA*
[23] *Department of Materials Science and Engineering, University of California, Berkeley, CA 94720 - USA*
[24] *Massachusetts Institute of Technology, Cambridge, MA 02139 - USA*
[25] *Physics Division, Lawrence Berkeley National Laboratory, Berkeley, CA 94720 - USA*
[26] *Laboratorio de Fisica Nuclear y Astroparticulas, Universidad de Zaragoza, Zaragoza 50009 - Spain*
[27] *Dipartimento di Scienze per la Qualità della Vita, Alma Mater Studiorum - Università di Bologna, Bologna I-47921 - Italy*
[28] *CEA, Centre de Saclay, Irfu/SPP, F-91191 Gif-sur-Yvette, France*
[29] *Lawrence Livermore National Laboratory, Livermore, CA 94550 - USA*
[30] *Department of Nuclear Engineering, University of California, Berkeley, CA 94720 - USA*
[31] *INFN - Sezione di Padova, Padova I-35131 - Italy*
[32] *Dipartimento di Fisica, Università di Firenze, Firenze I-50125 - Italy*
[33] *INFN - Sezione di Firenze, Firenze I-50125 - Italy*
[34] *Dipartimento di Fisica e Astronomia, Alma Mater Studiorum - Università di Bologna, Bologna I-40127 - Italy*

(Dated: October 2, 2015)

We report the results of a search for neutrinoless double-beta decay in a 9.8 kg·yr exposure of ^{130}Te using a bolometric detector array, CUORE-0. The characteristic detector energy resolution and background level in the region of interest are 5.1 ± 0.3 keV FWHM and $0.058 \pm 0.004\,(\text{stat.}) \pm 0.002\,(\text{syst.})$ counts/(keV·kg·yr), respectively. The median 90 % C.L. lower-limit half-life sensitivity of the experiment is 2.9×10^{24} yr and surpasses the sensitivity of previous searches. We find no evidence for neutrinoless double-beta decay of ^{130}Te and place a Bayesian lower bound on the decay half-life, $T^{0\nu}_{1/2} > 2.7 \times 10^{24}$ yr at 90 % C.L. Combining CUORE-0 data with the 19.75 kg·yr exposure of ^{130}Te from the Cuoricino experiment we obtain $T^{0\nu}_{1/2} > 4.0 \times 10^{24}$ yr at 90 % C.L. (Bayesian), the most stringent limit to date on this half-life. Using a range of nuclear matrix element estimates we interpret this as a limit on the effective Majorana neutrino mass, $m_{\beta\beta} < 270 - 760$ meV.

Neutrinoless double-beta ($0\nu\beta\beta$) decay is a hypothesized lepton-number-violating process [1] that has never been decisively observed. Its discovery would prove that lepton number is not a symmetry of nature, establish that neutrinos are Majorana fermions, possibly constrain the absolute neutrino mass scale, and support theories that leptons seeded the matter-antimatter asymmetry in the universe [2]. The clear potential for fundamental impact has motivated intense effort to search for this decay [3–5].

The Cryogenic Underground Observatory for Rare Events (CUORE) [6, 7], now in the final stages of construction at Laboratori Nazionali del Gran Sasso (LNGS), promises to be one of the most sensitive upcoming $0\nu\beta\beta$ decay searches. The detector exploits the bolometric technique [8, 9] in $5 \times 5 \times 5$ cm^3 $^{\text{nat}}TeO_2$ crystals, whereby the tiny heat capacity attained by a crystal at ∼10 mK results in a measurable increase of its temperature when it absorbs energy. The sought-after signature of $0\nu\beta\beta$ decay is a peak in the measured energy spectrum at the transition energy ($Q_{\beta\beta}$), which for ^{130}Te is 2527.518 ± 0.013 keV [10].

CUORE will consist of 19 towers containing 52 crystals each; CUORE-0 is one such tower built using the low-background assembly techniques developed for CUORE [11]. The 52 crystals [12] are held in an ultrapure copper frame by polytetrafluoroethylene supports and arranged in 13 floors, with 4 crystals per floor. Each crystal is instrumented with a neutron-transmutation-doped Ge thermistor [13] to record thermal pulses and a silicon heater to generate reference pulses [14]. The tower is deployed in Hall A of LNGS and exploits the cryogenic system, shielding configuration, and electronics from a predecessor experiment, Cuoricino [15–17].

CUORE-0 represents the state of the art for large-mass, low-background, ultra-low-temperature bolometer arrays. While also a competitive $0\nu\beta\beta$ decay search, it has validated the ultraclean assembly techniques and radiopurity of materials for the upcoming CUORE experiment. Technical details can be found in [11, 12, 18–20]; we focus here on the first physics results from CUORE-0.

The data were collected in twenty month-long blocks called *datasets* during two campaigns which ran from March 2013 to August 2013 and from November 2013 to March 2015. For approximately three days at the beginning and end of each dataset we calibrated the detector by placing thoriated wires next to the outer vessel of the cryostat. Data collected between calibrations, denoted *physics data*, are used for the $0\nu\beta\beta$ decay search.

Each thermistor voltage, except for one thermistor which we failed to wire bond, is continuously acquired at a rate of 125 Hz. Events are identified using a software trigger with a channel-dependent threshold of between 30 keV and 120 keV. The trigger rate per bolometer is 60 mHz (1 mHz) in calibration (physics) mode. Particle-induced pulses have rise (decay) times of ∼0.05 s (∼0.2 s), and have amplitudes of ∼0.3 μV/keV before amplification. We analyze a 5-s-long window consisting of 1 s before and 4 s after each trigger. The pre-trigger voltage establishes the bolometer temperature before the event; the pulse amplitude establishes the event energy. Every 300 s, a stable current pulse is injected in each heater to generate tagged monoenergetic reference pulses. Noise waveforms are collected on all bolometers every 200 s.

The analysis utilizes two pulse-filtering techniques, denoted optimal filter (OF) and decorrelated optimal filter (DOF), and two methods for thermal gain stabilization (TGS), denoted heater-TGS and calibration-TGS. The filters optimize energy resolution [21] by exploiting the distinct frequency characteristics of particle-induced vs. noise pulses. TGS corrects for small changes in the energy-to-amplitude response of the detection chain using monoenergetic heater or calibration events. Both OF and heater-TGS were used for Cuoricino [17]. We developed DOF to reduce correlated noise between adjacent crystals; such noise mainly affects the upper floors of the tower closest to cryostat noise sources [22, 23].

To recover data from the two bolometers with non-functioning heaters and from periods when temperature drifts in a bolometer exceeded the linear dynamic range of the heater-TGS, we developed calibration-TGS, which uses the 2615 keV ^{208}Tl calibration line. To successfully apply calibration-TGS to physics data, we monitor parameters that can affect the bolometer response between calibrations (e.g., drifts in DC offset or amplifier gain). Where possible we employ both TGS methods, yielding up to four stabilized pulse-amplitude estimators for each

* Present address: Physics Department, Princeton University, Princeton, NJ 08544, USA
† Deceased.

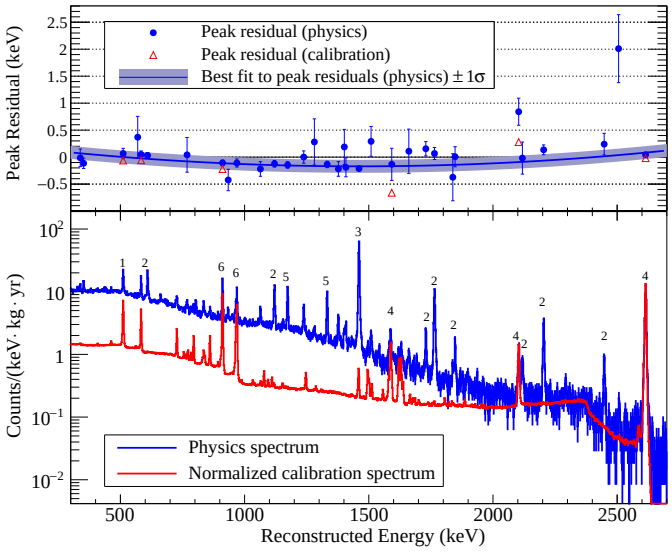

FIG. 1. Bottom: Energy spectra of physics (blue) and calibration (red) data; the latter is normalized relative to the former at 2615 keV. The peaks are identified as: (1) e^+e^- annihilation, (2) ^{214}Bi, (3) ^{40}K, (4) ^{208}Tl, (5) ^{60}Co, and (6) ^{228}Ac. Top: Difference of best-fit reconstructed peak energy and expected peak-energy for physics (blue points) and calibration (red) data. The blue line is the best-fit function to the physics peak residuals; the shaded band is its 1σ uncertainty.

event (OF and DOF, with heater- and calibration-TGS).

To convert these to energy, we correlate prominent peaks in the stabilized-amplitude spectra collected in calibration runs with gamma lines of known energy between 511 keV and 2615 keV (Fig. 1). We fit a quadratic function with zero intercept to the peak-mean vs. known-energy points to determine a calibration function for each stabilized-amplitude estimator of each bolometer-dataset and apply these to the physics data. To avoid biasing the subsequent analysis we then *blind* the physics data in the region of interest (ROI) using a procedure [24] which produces an artificial peak at $Q_{\beta\beta}$.

We select the best-performing energy estimator for each bolometer-dataset to optimize sensitivity to $0\nu\beta\beta$ decay (quantified by the ratio of energy resolution of the 2615 keV calibration line to the physics data exposure). While the combination of OF with heater-TGS is the default choice, combinations involving DOF and calibration-TGS — which are more robust against low-frequency common-mode noise and long-term temperature drifts, respectively — are selected if the improvement relative to the default is statistically significant. The fractions of exposure using OF with calibration-TGS, DOF with heater-TGS, and DOF with calibration-TGS are 21%, 12%, and 8%, respectively. These new techniques result in a 4% improvement in energy resolution and a 12% increase in usable exposure.

We select $0\nu\beta\beta$ decay candidates in the physics data according to the following conditions. First, we discard low-quality data (e.g., periods of cryostat instability or equipment malfunction), reducing the total exposure by 7%. To allow a bolometer time to equilibrate after each event (pileup rejection) we require that the times since the previous event and until the next event on the same bolometer are greater than 3.1 s and 4.0 s, respectively. To reject noisy pulses which can contribute to background we require each waveform to be consistent with a reference waveform, constructed for each bolometer-dataset from calibration data around the 2615 keV ^{208}Tl peak. Six pulse-shape parameters characterize the waveforms, and the acceptance criteria are tuned simultaneously on prominent peaks in the physics data to maximize the signal sensitivity at each peak. These peaks range in energy between 146 keV and 2615 keV. The sensitivity is quantified by the ratio of signal accepted to square-root of background accepted, where the signal sample is drawn from events that populate each peak and the background is drawn from nearby off-peak events. The tuning uses 50% of the data, randomly selected, and excludes the ROI. To reduce background from decays depositing energy in multiple crystals (e.g., α's at crystal surfaces or multiple Compton scatters) we reject an event if another occurs in the tower within ±5 ms (anticoincidence).

The selection efficiencies are evaluated with the fraction of data not used for tuning and averaged over all bolometer-datasets. The trigger efficiency is estimated from the fraction of heater pulses that produce an event trigger; we also exploit the heater events to measure the energy reconstruction efficiency (i.e., the probability for a monoenergetic pulse to reconstruct correctly). The combined trigger and reconstruction efficiency is $(98.529 \pm 0.004)\%$. The combined efficiency of the pileup and pulse-shape selection, estimated from the fraction of 2615 keV ^{208}Tl events in physics data that pass this selection, is $(93.7 \pm 0.7)\%$. The anticoincidence efficiency has two components: the probability for a $0\nu\beta\beta$ decay to be fully contained in one crystal and the probability for it to survive accidental coincidences. The former, estimated from simulation [25], is $(88.35 \pm 0.09)\%$; the latter we find to be $(99.64 \pm 0.10)\%$ using the 1461 keV γ-ray from ^{40}K. The total selection efficiency is $(81.3 \pm 0.6)\%$.

We use the high-statistics 2615 keV ^{208}Tl line in calibration data to establish the detector response to a monoenergetic deposit (lineshape) near the ROI. The data exhibit a slightly non-Gaussian lineshape characterized by a primary peak and a secondary peak whose mean is lower in energy by ∼0.3% and whose amplitude is typically ∼5% of the primary peak. Non-Gaussian low-energy structure was also observed in Cuoricino [26, 27]. The origin of this structure in CUORE-0 is under investigation. We studied several lineshapes, including double- and triple-Gaussian models; while the latter perform well at the ^{208}Tl line, we adopt the double-Gaussian lineshape as it is the simplest that reproduces the detector response over the broadest energy range.

We parametrize the lineshape ρ for each bolometer-dataset $(b,\ d)$ as $\rho_{b,d} = \rho(\mu_{b,d}, \sigma_{b,d}, \delta_{b,d}, \eta_{b,d})$. For each

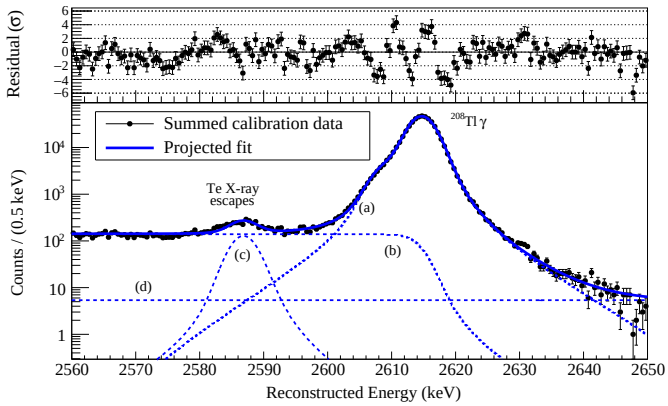

FIG. 2. Bottom: Calibration data near the 2615 keV ^{208}Tl γ-ray line, integrated over all bolometer-datasets. The solid blue line is the projection of the UEML fit described in the main text. In addition to the double-Gaussian lineshape for each bolometer-dataset, the fit function includes terms to model a multiscatter Compton continuum, a $\sim$30 keV Te X-ray escape peak, and a continuum background; these components, summed over all bolometer-datasets, are indicated by the blue dashed lines (a), (b), (c), and (d), respectively. Top: Normalized residuals of the data and the best-fit model.

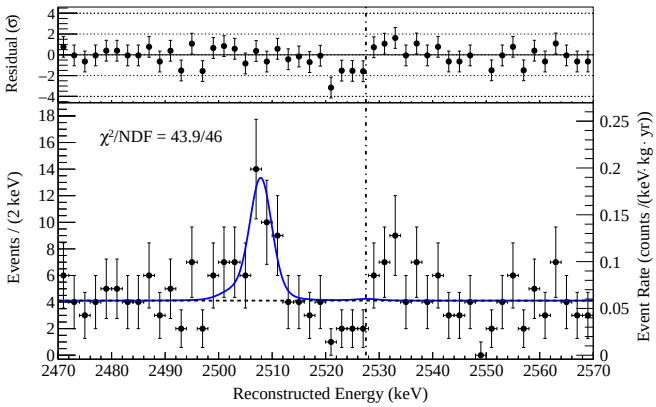

FIG. 3. Bottom: The best-fit model from the UEML fit (solid blue line) overlaid on the spectrum of $0\nu\beta\beta$ decay candidates in CUORE-0 (data points); the data are shown with Gaussian error bars. The peak at $\sim$2507 keV is attributed to ^{60}Co; the dotted black line shows the continuum background component of the best-fit model. Top: The normalized residuals of the best-fit model and the binned data. The vertical dot-dashed black line indicates the position of $Q_{\beta\beta}$.

(b, d) pair, $\mu_{b,d}$ is the mean of the primary peak, $\delta_{b,d}$ is the ratio of the means of the secondary and primary peaks, $\sigma_{b,d}$ is the common Gaussian width of both peaks, and $\eta_{b,d}$ is the fractional intensity of the secondary peak. We estimate these parameters with a simultaneous, unbinned extended maximum likelihood (UEML) fit to the 2615 keV ^{208}Tl calibration line (Fig. 2); the resulting best-fit parameters are denoted $\hat{\mu}_{b,d}$, $\hat{\sigma}_{b,d}$, $\hat{\delta}_{b,d}$, and $\hat{\eta}_{b,d}$.

We next repeat this lineshape fit on a series of peaks of known energy between 511 keV and 2615 keV in the physics data (Fig. 1). For a peak of known energy E, $\mu_{b,d}(E)$ can vary around the expected calibrated energy via a single free parameter $\Delta\mu(E)$. To treat energy dependence of the resolution or possible differences in resolution between calibration vs. physics data, we vary the $\sigma_{b,d}$ relative to $\hat{\sigma}_{b,d}$ via a global scaling parameter $\alpha_\sigma(E)$. We fix the $\delta_{b,d}$ and $\eta_{b,d}$ to the corresponding $\hat{\delta}_{b,d}$ and $\hat{\eta}_{b,d}$.

The energy residual parameters $\Delta\mu(E)$ are plotted in Fig. 1. A prominent outlier is the peak attributed to ^{60}Co double-gamma events which reconstructs at 2507.6 ± 0.7 keV, 1.9 ± 0.7 keV higher than expected [28]; a shift of 0.8 ± 0.3 keV was observed in Cuoricino [26]. The single-escape peak of the ^{208}Tl 2615 keV gamma at 2104 keV also reconstructs higher by 0.84 ± 0.22 keV. Data taken with a ^{60}Co source confirm the double-gamma events reconstruct at higher energy, in agreement with our physics data. Simulations show their energy deposit in a bolometer is less localized than the single-gamma lines studied; this may be responsible for the observed response. The double-escape peak of the ^{208}Tl 2615 keV line ($E\simeq1593$ keV) reconstructs within 0.13 ± 0.30 keV of the expected value. Since e^+e^- pairs and $0\nu\beta\beta$ decays share similar event topologies we assume the latter would reconstruct according to the calibrated energy scale.

We estimate the calibration offset at $Q_{\beta\beta}$ from a parabolic fit to the physics-peak residuals in Fig. 1, excluding the ^{60}Co double-gamma and ^{208}Tl single-escape lines as outliers. We adopt the standard deviation of the parabolic-fit residuals as a systematic uncertainty. The result is $\Delta\mu(Q_{\beta\beta}) = 0.05\pm0.05(\text{stat.})\pm0.09(\text{syst.})$ keV. Similarly, fitting the resolution-scaling parameters with a linear function we find $\alpha_\sigma(Q_{\beta\beta}) = 1.05\pm0.05$. Using this $\alpha_\sigma(Q_{\beta\beta})$, we estimate from calibration data the FWHM at $Q_{\beta\beta}$ of each bolometer-dataset in physics data. We quote the exposure-weighted harmonic mean of these physics FWHM values, 5.1 ± 0.3 keV, as a characteristic value of the detector resolution in the ROI [23]. The RMS of the calibration FWHM values is 2.9 keV.

After unblinding the ROI by removing the artificial peak, we determine the yield of $0\nu\beta\beta$ decay events from a simultaneous UEML fit [26] in the energy region 2470–2570 keV (Fig. 3). The fit components are: a posited signal peak at $Q_{\beta\beta}$, a peak at $\sim$2507 keV from ^{60}Co double-gammas, and a continuum background attributed to multiscatter Compton events from ^{208}Tl and surface decays [29]. We model both peaks using the established lineshape. For $0\nu\beta\beta$ decay, the $\mu_{b,d}(Q_{\beta\beta})$ are fixed at the expected position (i.e., 87.00 keV $-\,\Delta\mu(Q_{\beta\beta})$ below $\hat{\mu}_{b,d}$, where 87.00 keV is the nominal energy difference between $Q_{\beta\beta}$ and the ^{208}Tl line), the $\sigma_{b,d}$ are fixed to be $1.05\times\hat{\sigma}_{b,d}$, the $\delta_{b,d}$ and $\eta_{d,b}$ are fixed to their best-fit calibration values, and the $0\nu\beta\beta$ decay rate ($\Gamma_{0\nu}$) is treated as a global free parameter. The ^{60}Co peak is treated in a similar way except that a global free parameter is added to the expected $\mu_{b,d}$ to accomodate the anomalous double-gamma reconstruction. The ^{60}Co yield, although a free parameter, is constrained to follow the isotope's

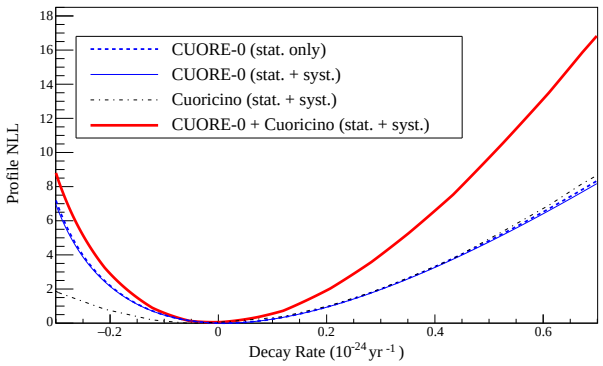

FIG. 4. Profile negative log-likelihood (NLL) curves for CUORE-0, Cuoricino [15–17], and their combination.

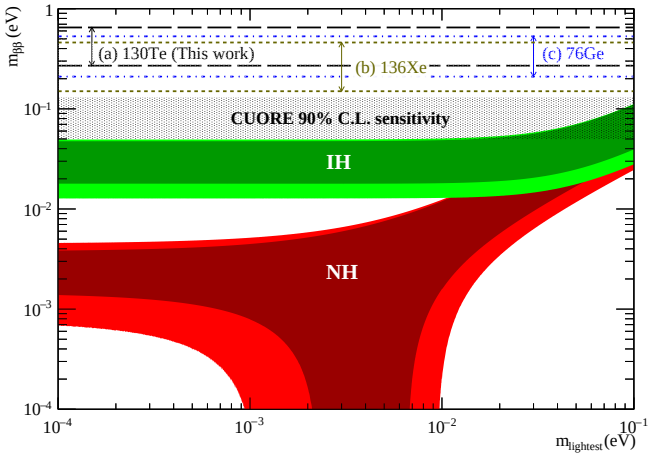

FIG. 5. Constraints on $m_{\beta\beta}$ vs. lightest neutrino mass (m_{lightest}). For the inverted (IH, green) and normal (NH, red) hierarchies the central dark band is derived from the best-fit neutrino oscillation parameters, the lighter outer band includes their 3σ uncertainties [39]. The horizontal bands delineated by the long-dashed black lines (a), the dashed beige lines (b), and the dot-dashed blue lines (c) are the range of 90% C.L upper limits on $m_{\beta\beta}$ coming from (a)^{130}Te (CUORE-0 combined with Cuoricino), (b)^{136}Xe (EXO-200 [40], KamLAND-Zen [41] independently), and (c)^{76}Ge (combined limit from Gerda, IGEX, HDM [42]). The vertical arrows aim to emphasize the range currently probed with each isotope. The horizontal, hashed grey band indicates the range of limits on $m_{\beta\beta}$ expected from CUORE assuming its target 90%C.L lower limit half-life sensitivity of 9.5×10^{25} yr is attained.

half-life [28] since it was cosmogenically produced above ground but is not replenished under ground at LNGS. Within the limited statistics the continuum background can be modeled with a zeroth-order polynomial; we consider first- and second-order alternatives later.

The ROI contains 233 candidates in a total exposure of 35.2 kg·yr of TeO_2, or 9.8 kg·yr of ^{130}Te considering the natural isotopic abundance of 34.167% [30]. The best-fit $\Gamma_{0\nu}$ is $0.01 \pm 0.12\,(\text{stat.}) \pm 0.01\,(\text{syst.}) \times 10^{-24}$ yr^{-1}, and the best-fit background index in the ROI is $0.058 \pm 0.004\,(\text{stat.}) \pm 0.002\,(\text{syst.})$ counts/(keV·kg·yr).

We evaluate the goodness of fit by comparing the value of the binned χ^2 in Fig. 3 (43.9 for 46 degrees of freedom) with the distribution from a large set of pseudo-experiments with 233 Poisson-distributed events in each, and generated with the best-fit values of all parameters; 90% of trials return $\chi^2 > 43.9$. The data are also compatible with this set of pseudo-experiments according to the Kolmogorov-Smirnov metric. We quantify the significance of each of the positive and negative fluctuations about the best-fit function by comparing the likelihood of our best-fit model to the likelihood from an UEML fit where the fluctuation is modeled with a signal peak. For one degree of freedom, the most negative (positive) fluctuation has a probability of 0.5% (3%). The probability to realize the largest observed fluctuation anywhere in the 100-keV ROI is $\sim 10\%$.

We find no evidence for $0\nu\beta\beta$ decay and set a 90% C.L. Bayesian upper limit at $\Gamma_{0\nu} < 0.25 \times 10^{-24}$ yr^{-1}, or $T^{0\nu}_{1/2} > 2.7 \times 10^{24}$ yr (statistical uncertainties only); the prior used was uniform ($\pi(\Gamma_{0\nu}) = 1$ for $\Gamma_{0\nu} >= 0$). The median 90% C.L. lower-limit sensitivity for $T^{0\nu}_{1/2}$ is 2.9×10^{24} yr. The probability to obtain a more stringent limit than the one reported above is 54.7%. Including systematic uncertainties (Table I) the 90% C.L. limits are $\Gamma_{0\nu} < 0.25 \times 10^{-24}$ yr^{-1} or $T^{0\nu}_{1/2} > 2.7 \times 10^{24}$ yr.

To estimate systematic uncertainties we perform a large number of pseudo-experiments with zero and non-zero signals. We find the bias on $\Gamma_{0\nu}$ from the UEML analysis is negligible. To estimate the systematic error of the lineshape choice we repeat the analysis of each pseudo-experiment with single- and triple-Gaussian models and study the deviation of the best-fit decay rate from the posited decay rate as a function of the latter. Similarly, we propagate the 5% uncertainty on $\alpha_\sigma(Q_{\beta\beta})$, the 0.09 keV energy scale uncertainty, and the choice of zeroth-, first-, or second-order polynomial for the background.

TABLE I. Systematic uncertainties on $\Gamma_{0\nu}$ for zero signal (Additive) and as a percentage of nonzero signal (Scaling).

	Additive (10^{-24} yr^{-1})	Scaling (%)
Lineshape	0.004	1.3
Energy resolution	0.006	2.6
Fit bias	0.006	0.15
Energy scale	0.006	0.4
Bkg function	0.004	0.7
Selection efficiency	0.7%	

We combine our data with a 19.75 kg·yr exposure of ^{130}Te from Cuoricino [17]. The exposure-weighted mean and RMS FWHM energy resolution of the detectors were 6.9 keV and 2.9 keV, respectively; the ROI background index was 0.169 ± 0.006 counts/(keV·kg·yr). We report the profile likelihoods in Fig. 4. The combined Bayesian

90% C.L. limit is $T^{0\nu}_{1/2} > 4.0 \times 10^{24}$ yr, which is the most stringent limit to date on this quantity. For comparison, the 90% C.L. frequentist limits [31] are $T^{0\nu}_{1/2} > 2.8 \times 10^{24}$ yr for CUORE-0 only, and $T^{0\nu}_{1/2} > 4.1 \times 10^{24}$ yr for the combination with Cuoricino.

We interpret our Bayesian combined limit in the context of models for $0\nu\beta\beta$ decay mediated by light Majorana neutrino exchange using the phase-space factors from [32], the most recent nuclear matrix element (NME) calculations for a broad range of models [33–37], and assuming $g_A \simeq 1.27$ for the axial coupling constant. The resulting range for the 90% C.L. upper limit on the effective Majorana mass is $m_{\beta\beta} < 270 - 650$ meV; for ease of comparison with limits from other isotopes in the field (Fig. 5) this range excludes Ref. [38]. Including the latter NME, the range extends to $m_{\beta\beta} < 270 - 760$ meV.

In summary, CUORE-0 finds no evidence for $0\nu\beta\beta$ decay of ^{130}Te and, when combined with Cuoricino, achieves the most stringent limit to date on this process. Benefiting from lower background, improved energy resolution, and higher data-taking efficiency, CUORE-0 surpassed the sensitivity of Cuoricino in half the runtime.

The CUORE Collaboration thanks the directors and staff of the Laboratori Nazionali del Gran Sasso and our technical staff for their valuable contribution to building and operating the detector. The authors thank J. Feintzeig, L. Gladstone, P. Mosteiro, and V. Singh for carefully reviewing the manuscript, M. Nastasi for preparing the ^{60}Co calibration sources, and F. Iachello for helpful discussions concerning the NME literature. This work was supported by the Istituto Nazionale di Fisica Nucleare (INFN); the National Science Foundation under Grant Nos. NSF-PHY-0605119, NSF-PHY-0500337, NSF-PHY-0855314, NSF-PHY-0902171, NSF-PHY-0969852, NSF-PHY-1307204, and NSF-PHY-1404205; the Alfred P. Sloan Foundation; the University of Wisconsin Foundation; and Yale University. This material is also based upon work supported by the US Department of Energy (DOE) Office of Science under Contract Nos. DE-AC02-05CH11231 and DE-AC52-07NA27344; and by the DOE Office of Science, Office of Nuclear Physics under Contract Nos. DE-FG02-08ER41551 and DE-FG03-00ER41138. This research used resources of the National Energy Research Scientific Computing Center (NERSC).

[1] B. Pontecorvo, Sov. Phys. JETP **26**, 984 (1968).
[2] M. A. Luty, Phys. Rev. D **45**, 455 (1992).
[3] A. Giuliani, A. Poves, Advances in High Energy Physics **2012**, 857016, (2012).
[4] O. Cremonesi, M. Pavan, Advances in High Energy Physics, **2014**, 951432, (2014).
[5] A. S. Barabash, Phys. Usp. **57**, 482 (2014).
[6] C. Arnaboldi *et al.*, [CUORE Collaboration], Nucl. Instrum. Meth. A **518**, 775 (2004).
[7] R. Ardito *et al.*, [CUORE Collaboration], hep-ex/0501010 .
[8] E. Fiorini and T. O. Niinikoski, Nuclear Instruments and Methods in Physics Research **224**, 83 (1984).
[9] C. Enss, D. McCammon, J. Low Temp Phys **151**, 5, (2008).
[10] M. Redshaw *et al.* Phys. Rev. Lett. **102**, 212502 (2009).
[11] E. Buccheri *et al.*, Nucl. Instrum. Meth. A **768**, 130 (2014).
[12] C. Arnaboldi *et al.*, J. Cryst. Growth **312**, no. 20, 2999 (2010).
[13] E. E. Haller *et al.*, Neutron Transmutation Doping of Semiconductor Materials, Springer US, 1984.
[14] E. Andreotti *et al.*, Nucl. Instrum. Meth. A **664**, 161 (2012).
[15] C. Arnaboldi *et al.*, Phys. Lett. B **584**, 260 (2004).
[16] C. Arnaboldi *et al.*, Phys. Rev. C **78**, 035502 (2008).
[17] E. Andreotti *et al.*, Astropart. Phys. **34**, 822 (2011).
[18] Article in preparation [CUORE Collaboration] .
[19] F. Alessandria *et al.*, Astropart. Phys. **35**, 839 (2012).
[20] F. Alessandria *et al.*, Astropart. Phys. **45**, 13 (2013).
[21] E. Gatti,P .F. Manfredi, Riv. Nuovo Cimento **9**, 1 (1986).
[22] C. Mancini-Terracciano and M. Vignati, JINST **7**, P06013 (2012).
[23] J. L. Ouellet Ph.D. thesis, University of California, Berkeley, 2015 .
[24] D. R. Artusa *et al.*, Eur. Phys. J. C **74**, no. 8, 2956 (2014).
[25] S. Agostinelli *et al.*, [GEANT4 Collaboration], Nucl. Instrum. Meth. A **506**, 250 (2003); release v4.9.6.p03 with the Livermore physics list .
[26] A. Bryant Ph.D. thesis, University of California, Berkeley, 2010 .
[27] M. Carrettoni Ph.D. thesis, Università Degli Studi Di Milano Bicocca, 2011
[28] National Nuclear Data Center, www.nndc.bnl.gov .
[29] Article in preparation [CUORE Collaboration]
[30] M. A. Fehr *et al.* Int. J. Mass Spectrom. **232** (1), 83 (2004).
[31] W.Rolke et *al.*, Nucl. Instrum. Meth. A **551**, 493-503 (2005).
[32] J. Kotila and F. Iachello, Phys. Rev. C **85**, 034316 (2012).
[33] J. Menendez *et al.*, Nucl. Phys. A **818**, 139 (2009).
[34] F. Ŝimkovic et *al.*, Phys. Rev. C **87**, 045501 (2013).
[35] J. Barea *et al.* Phys. Rev. C **91**, 034304 (2015).
[36] T. R. Rodriguez and G. Martinez-Pinedo, Phys. Rev. Lett. **105**, 252503 (2010).
[37] J. Hyvrinen and J. Suhonen, Phys. Rev. C **91**, 024613 (2015).
[38] A. Neacsu and M. Horoi, Phys. Rev. C **91**, 024309 (2015).
[39] K. A. Olive *et al.* (Particle Data Group), Chin. Phys. C, **38**, 090001 (2014).
[40] J. B. Albert *et al.* [EXO-200 Collaboration], Nature **510**, 229 (2014)
[41] A. Gando *et al.* [KamLAND-Zen Collaboration], Phys. Rev. Lett. **110**, no. 6, 062502 (2013)
[42] M. Agostini *et al.* [GERDA Collaboration], Phys. Rev. Lett. **111**, no. 12, 122503 (2013)